Does a Morphological Adjustment during Tsunami Inundation Increase Levels of Hazards?

B. Tehranirad[1]; J. T. Kirby[2]; S. T. Grilli[3]; and F. Shi[4]

[1]Center for Applied Coastal Research, Univ. of Delaware, Newark, DE, USA
[2]Center for Applied Coastal Research, Univ. of Delaware, Newark, DE, USA
[3]Dept. of Ocean Engineering, Univ. of Rhode Island, Narragansett, RI, USA
[4]Center for Applied Coastal Research, Univ. of Delaware, Newark, DE, USA

ABSTRACT

Tsunamis are able to move large amounts of sediment during their inundation process. However, previous studies conducted to assess tsunami hazard have not considered tsunami-induced sediment transport in their simulations, although it is possible that morphological adjustments during tsunami inundation increase the levels of hazard. In this paper, we present a model which is able to simulate sediment processes caused by tsunami action. The model is validated by comparing results to an experiment of sediment transport under breaking solitary waves. Finally, the model is applied to the simulation of sediment transport over a typical barrier island geometry, and we study the resulting changes in tsunami runup on the mainland behind the barrier, as compared to fixed bathymetry/topography conditions. We show that considering morphological changes during tsunami inundation modeling can increase the runup on the mainland behind the barrier. We conclude that assuming a fixed bathymetry when modeling tsunami coastal hazard may lead to underestimating runup and inundation values and cause errors in estimating the tsunami inundation line.

Keywords: Tsunami; Sediment Transport; US East Coast Tsunami Hazard

INTRODUCTION

A tsunami can significantly change coastal morphology. Post-tsunami surveys have shown that large amounts of sediment can be moved in bays and estuaries by tsunami action, especially over coastal dunes (Tanaka et al., 2012; Goto et al., 2012; Udo et al., 2012; Szczuciński et al., 2012). During tsunami inundation, large amounts of sediment have been eroded from sandy coasts and deposited further onshore (Wilson et al., 2012). In some cases, sand dunes have been completely eroded by a tsunami, with the eroded sediment being deposited either onshore behind the dunes, or offshore during the rundown process (Goto et al., 2012). Field surveys conducted after the 2004 Indian

Ocean Tsunami have identified tsunami deposits extending 1 km inland in low-lying coastal areas of the western coast of Thailand, where the sand origin was the coastal dunes that skirted the original shoreline (Choowong et al., 2008; Hori et al., 2007). Similar erosion-deposition patterns were observed in different locations following the 2011 Tohoku-Oki tsunami (Udo et al., 2012; Goto et al., 2012)).

Although tsunamis are known to cause significant sediment motion, particularly along sandy coasts, models used for simulating coastal tsunami hazard do not typically consider bathymetric changes caused by erosion and deposition during simulations. In some studies, the elevation of coastal dunes has been arbitrarily lowered before computing tsunami inundation, in order to obtain safe estimates of tsunami impact on critical coastal infrastructures. However, the ability of a tsunami to significantly reshape the morphology of sandy coasts during the inundation phase

requires a more careful and site-specific analysis of how such changes may increase the level of coastal hazard and inundation. This could be critical in many areas of the United States (US) East Coast, which features numerous sandy coasts and barrier islands, where the authors have been performing inundation mapping for the past 5 years under the auspices of the US National Tsunami Hazard Mitigation Program (NTHMP), considering fixed bathymetry conditions.
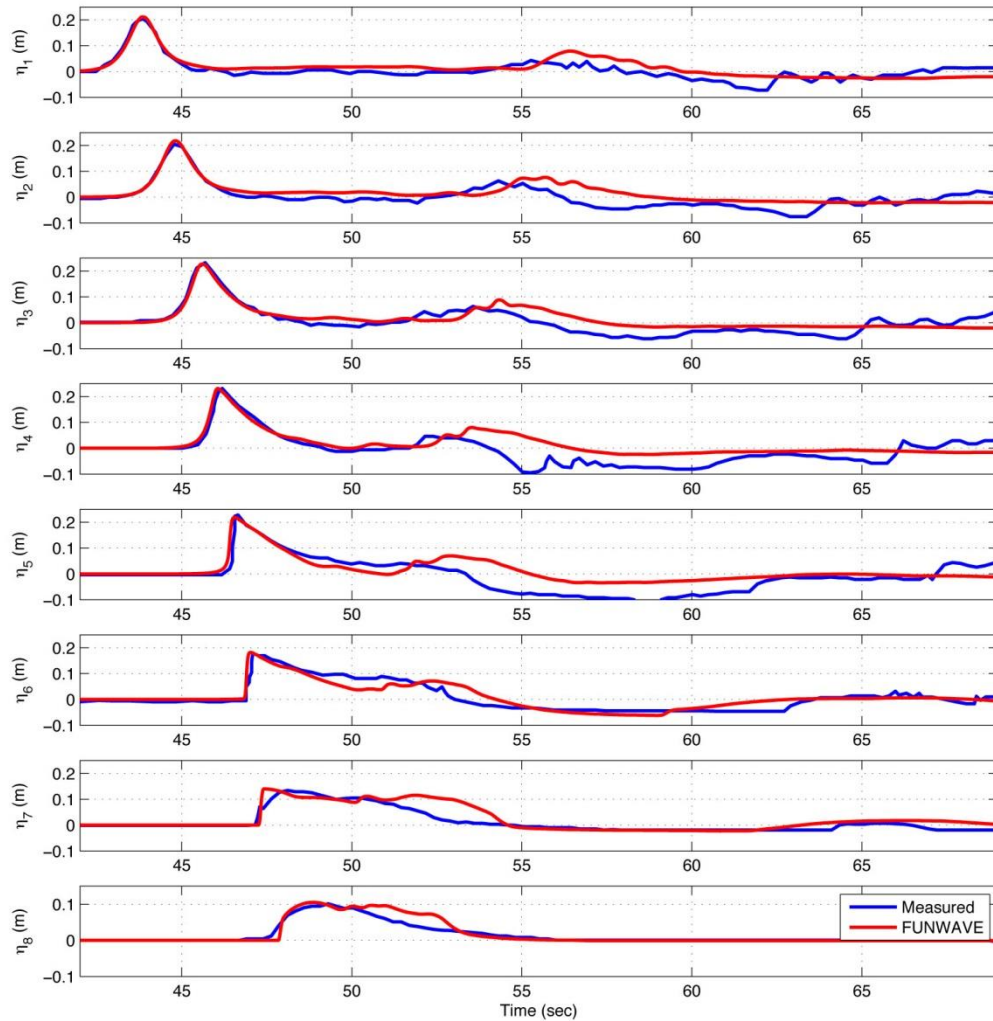

Figure 1: Comparison between measured (Blue line) and simulated (Red line) surface elevations at eight different gauges, for the fourth solitary wave in a sequence of 8 waves. Laboratory experiments by Kobayashi and Lawrence (2004).

In this NTHMP work, we model maximum inundation from the largest Probable Maximum Tsunamis (PMTs) in the Atlantic Ocean basin and margin. These included tsunamis generated by: (i) two M9 coseismic sources in the Gibraltar convergence zone (GCZ) (Grilli and Grilli, 2013) and in the Puerto Rico Trench (PRT) (Grilli et al., 2010); (ii) large flank collapses of the Cumbre Vieja volcano (CVV), on La Palma in the Canary Islands, with different slide sizes (Tehranirad et al., 2015); and (iii) near-field submarine mass failures (SMFs) on the continental shelf break (Grilli et al., 2014). Results showed that many communities protected by barrier islands, such as Atlantic City, NJ, Ocean City, MD, and the southern coast of Long Island, NY, would be among the most affected shorelines. Simulations showed that most of these barrier

islands would be completely overtopped by one of these major tsunamis, causing large velocities over the barrier crests and suggesting that significant topographic changes could potentially occur in the barrier areas. In this study, we have tried to assess whether such barriers would be significantly eroded during tsunami impact to increase runup and inundation on the mainland, behind the barrier, as compared to fixed bathymetry conditions such as we have assumed so far.
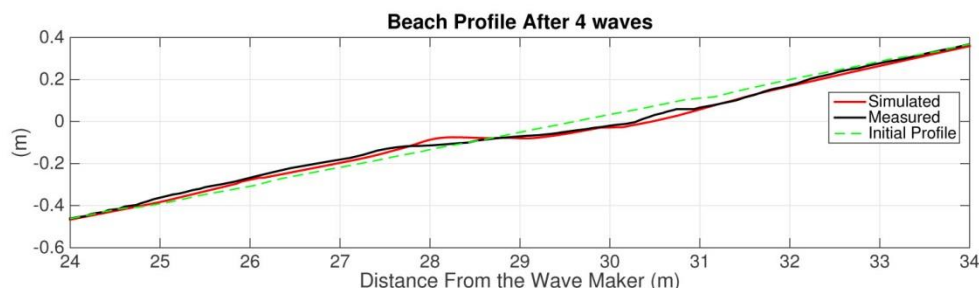

Figure 2: Comparison between measured (Black line) and simulated (Red line) beach profiles after 4 sequences of solitary waves in experiments by Kobayashi and Lawrence (2004).

To study tsunami-induced morphological changes, we coupled a sediment transport and morphology sub-model to our long wave tsunami propagation model FUNWAVE-TVD (Tehranirad et al., 2011; Shi et al., 2012; Kirby et al., 2013). After presenting details of this coupled model, we validate it by simulating experiments by Kobayashi and Lawrence (2004) for sediment transport under breaking solitary waves. Then, we apply the model to simulating tsunami-induced morphological changes over a typical US East Coast barrier topography, for three different PMT impacts. We show that runup values on the mainland behind the barrier could increase as a result of erosion of the barrier crest, demonstrating the importance of including real time morphological changes during tsunami simulation of coastal hazard and inundation.

GOVERNING EQUATIONS

We simulate tsunami propagation, coastal impact and inundation using FUNWAVE-TVD, a fully nonlinear Boussinesq model, usiung a series of one-way coupling of nested grids (both spherical and Cartesian) of increasing resolution toward the coast. FUNWAVE-TVD is coupled to a classical sediment transport and morphology submodel based on a convection-diffusion transport equation for the depth-averaged sediment concentration (C), with sediment pick-up (*P*) and deposition (*D*) functions (Elder, 1959), forced by the depth-averaged velocities (U,V) and total water depth ($d = h + \eta$) values computed for the incident tsunami.

$$\frac{\partial(Cd)}{\partial t} + \frac{\partial(Cq_x)}{\partial x} + \frac{\partial(Cq_y)}{\partial y} = \frac{\partial}{\partial x}\left(K_x d \frac{\partial C}{\partial x}\right) + \frac{\partial}{\partial y}\left(K_y d \frac{\partial C}{\partial y}\right) + P - D \qquad (1)$$

where $q_{x,y}$ are flow rates per unit width in the *x* and *y* directions (*Ud*, *Vd*), $K_{x,y}$ are sediment diffusion coefficients, *P* is a pickup function modeled following van Rijn (1984), *D* is a deposition function dependent on sediment grain fall velocity and on reference sediment concentration. Eq. 1 is solved using a finite difference scheme using the same time step as the hydrodynamic model. Resulting depth changes are then computed by averaging values of the pickup and deposition rates over a larger time step (usually between 5 and 20 times larger) to give

$$\frac{dh}{dt} = \frac{1}{n}(\bar{P} - \bar{D}) \tag{2}$$

where h is the still water depth, n is the sediment porosity, and $\bar{P}$ and $\bar{D}$ are the time-averaged pickup and deposition rates. The maximum seafloor slope is limited by using an avalanche scheme in the model (Larson and Kraus, 1989). When the beach slope exceeds the repose angle of the sediment, avalanching occurs and forms a new slope with the repose angle.
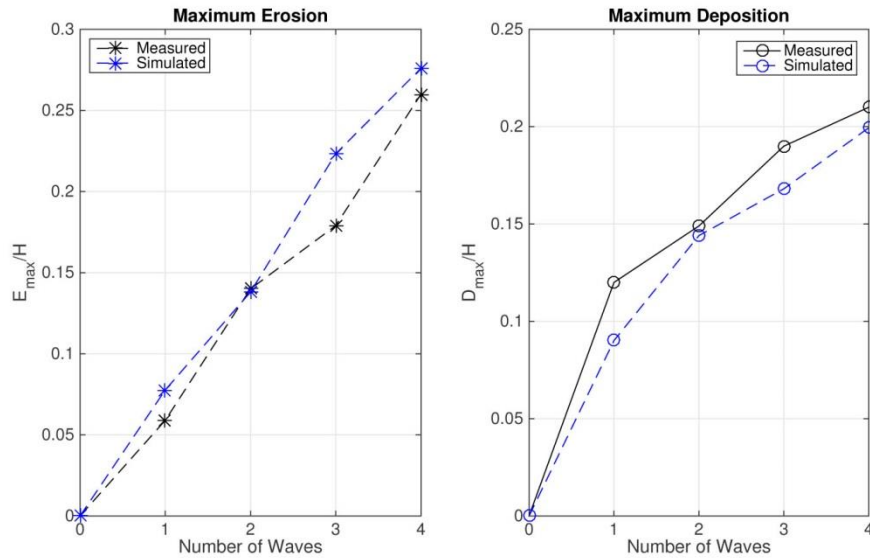

Figure 3: Comparison between measured maximum erosion (E_{max}) and deposition (D_{max}) for 4 sequences of solitary waves, normalized by wave height (H) in experiments by Kobayashi and Lawrence (2004).
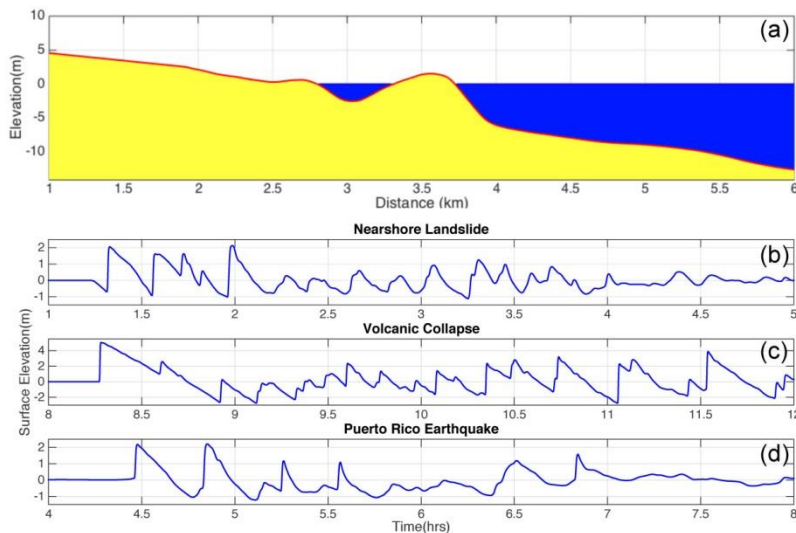

Figure 4: (a) Computational domain and one-dimensional bathymetry/topography used to simulate barrier island morphological changes during tsunami impact in Ocean City, MD. (b, c, d) Time series of surface elevations (time is from the start of each event) simulated with FUNWAVE-TVD and used as offshore (rightward) boundary conditions in the coupled model, for three PMTs caused by a SMF/landslide tsunami, a 450 km³ flank collapse of the CVV, and a M9 earthquake in the PRT, respectively.
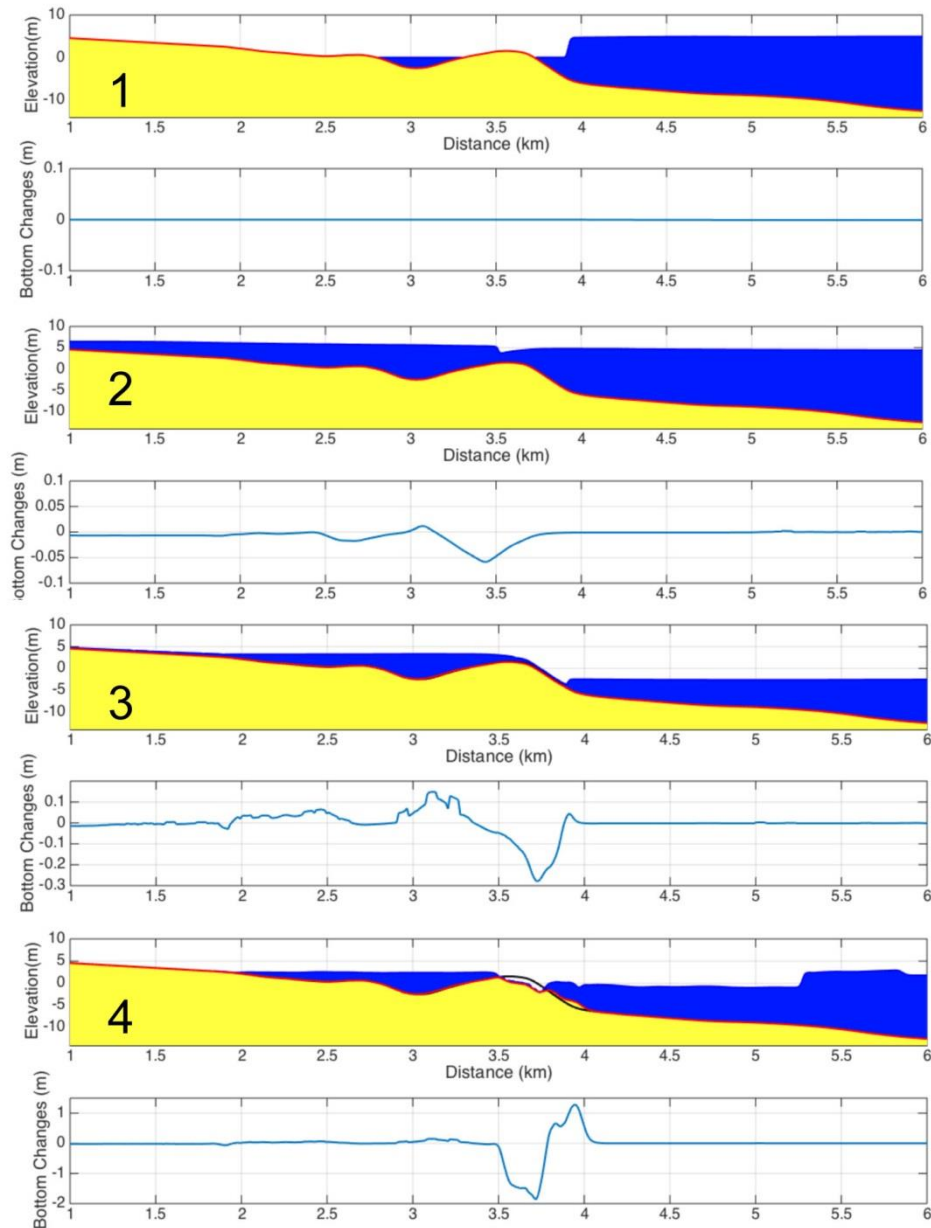
Figure 5: Different phases of tsunami-induced sediment transport over a barrier island off of Ocean City, MD, for the leading wave of the CVV flank collapse PMT (Fig. 4c). 1) Tsunami wave attack the barrier while negligibly eroding the shoreface. 2) Tsunami waves overtop the barrier; flow direction is onshore and sediment gets eroded from the top of the barrier and deposited in the back bay. 3) Tsunami waves rush down, causing massive erosion on the barrier shoreface. 4) The eroded sediment gets deposited offshore, causing sand dunes to be flatter. The blue lines under each figure show the net change in the bottom profile.

MODEL VALIDATION

Kobayashi and Lawrence (2004) conducted laboratory experiments to examine cross-shore sediment transport under breaking solitary waves on a fine sand beach, using a 30 m long, 2.4 m

wide, and 1.5 m deep wave tank. Waves were generated by a piston wave maker in 0.8 m depth, and a fine sand beach with an initial slope of 1/12 was built at the extremity of the tank. They recorded bed evolution as well as surface elevation and velocity at 8 locations, for a sequence of 8 solitary waves. The first gauge was located at the toe of the slope, while gauges 2-5 measured the solitary wave shoaling and breaking over the slope. Gauges 6-8 were located onshore to measure wave runup and rundown in the swash zone. The sand was well sorted with median diameter $d_{50} = 0.18$ mm, porosity $n = 0.4$, specific gravity $s = 2.6$, and fall velocity $V_f = 2.0$ cm/s. Here, we modeled sediment transport and bed changes for the first four waves and compared results to the measured laboratory data. The recorded initial wave height was $H_o = 0.216$ m, and we used a grid size of 5 cm to model wave propagation onshore. Figure 1 compares the measured and simulated surface elevations for the fourth solitary wave in the sequence, and shows a good agreement between model and experiment.

Figure 2 shows the comparison between measured and simulated beach profiles after 4 solitary waves. The major change in the bottom profile occurred during wave rundown, while the sand was eroded from the shoreline area and deposited further offshore. This process was observed during the experiment, and the model successfully captures this behavior. As shown in the figure, the model provides a good estimate of the location and magnitude of shoreline erosion. However, the location of the deposited sand is not simulated as well as that of the eroded sediment. Figure 3 shows the comparison between measured and simulated maximum deposition and erosion values for the first four waves in the experiment. The model is seen to slightly overpredict erosion near the original shoreline. Overall, the model was able to predict bottom morphological changes with good agreements. After four sequences of solitary waves, the averaged point to point error of simulation results was 13 percent from measured bottom profile.

RESULTS

In the previous section, we showed that the proposed hydrodynamic-morphological change model is able to simulate morphological changes induced over a plane sandy beach by a train of solitary waves reasonably well. Here, the model is applied to simulate tsunami-induced morphological changes during impact over a barrier island located close to Ocean City, MD. To simplify this test case to a one-dimensional bathymetry, along-shore variations were eliminated by averaging several cross-sections of the beach profile in NOAA's Ocean City 1/3 arc-sec DEM (Grothe et al., 2010) to obtain the single profile shown in Figure 4. Surface elevations and horizontal velocity values simulated off of Ocean City in earlier NTHMP's tsunami inundation mapping, for three incident tsunamis, were used in the model as boundary conditions (Figures 4b,c,d) (Tehranirad et al., 2014) . The three tsunami sources studied here are: (i) a nearshore SMF; (ii) a 450 km^3 CVV flank collapse; and (iii) a M9 earthquake in the Puerto Rico trench (PRT). The process of modeling these sources is detailed in Grilli et al. (2010) and Tehranirad et al. (2015) for far-field sources and in Grilli et al. (2014) for near-field SMFs. Data simulated with FUNWAVE-TVD at a numerical wave gauge located off of Ocean

City's shoreline at depth of 12m was used to generate the offshore boundary condition in the coupled model grid, for the domain shown in Figure 4a. Figure 4b shows that, nearshore, the SMF/landslide tsunami consists of 3-4 larger waves of similar height followed by a dispersive train of smaller waves; by contrast, for the other two sources there are 1 or 2 larger waves in the beginning of the tsunami wave train, followed by smaller waves and then again by larger waves (Figure 4c,d). The grid resolution in the model was 1/3 arc-sec (about 10 m). For this analysis,

the sediment was assumed to be a fine quartz sand with $d_{50} = 0.2$ mm. No attempt was made to account for vegetation or a constructed environment.

Figure 5 shows different phases of tsunami-induced sediment movement for the leading wave of the CVV flank collapse PMT (Fig. 4c). For this and subsequent waves in the tsunami wave train, the process can be divided into four phases detailed in the figure. First, the tsunami bore approaches the barrier, while slightly eroding the shoreface. Then, the barrier is overtopped, and sediment erodes from the top of the barrier and deposits in the back bay. Next, while surface elevation drops nearshore during downrush, the flood water in the back bay starts flowing back into the ocean, creating critical flow conditions on the beach face. The largest erosion is caused during this phase. This is analogous to field observations citepgoto12, which suggest that the largest erosion caused by tsunamis occurs during the rundown process. Finally, before the second larger wave in the tsunami wave train reaches the shoreline, the eroded sediment from the barrier shoreface is deposited further offshore. This process causes the barrier to become flatter; therefore, the second wave (not shown here) will be less dissipated during the overtopping process as compared to fixed bathymetry conditions. Thus, larger waves will reach into the back bay, generating larger runup and inundation values on the mainland behind the barrier. For the CVV flank collapse and PRT sources, results of the coupled model show that tsunami runup values on the mainland are increased by about 4 percent. However, for the SMF source runup on the mainland behind the barrier is increased by 12 percent. This is because landslide tsunami signal is made of several similar larger waves (Fig. 4a), while the first 1-2 waves were significantly larger than later waves for the other two sources.

CONCLUDING REMARKS

In this paper, we showed that tsunamis are able to move large amounts of sediment, thereby reducing shoreline protection and increasing tsunami inundation as compared to a fixed bathymetry/topography. In order to account for morphological adjustments during tsunami inundation, we have coupled a hydrodynamic model (FUNWAVE-TVD) with sediment transport and morphology change models to simulate tsunami-induced sediment transport over a barrier island. The model was validated against laboratory data for sediment transport under breaking solitary waves. Then, using the new model, morphological changes were simulated for a typical US East Coast barrier island for three different tsunami sources, a landslide on the edge of the shelf break, a volcanic flank collapse in the Canary Islands, and an earthquake in the Puerto Rico Trench. Results showed that morphological adjustments during tsunami inundation may cause an increase in tsunami runup and inundation on the mainland behind the barrier, thus increasing the level of hazard. Although our preliminary one-dimensional simulation results off of Ocean City, MD, show that considering bottom changes alters the location of the tsunami inundation line as compared to a fixed bathymetry, we cannot draw general conclusions based only on such simplified simulations. In future work, we will model tsunami-induced morphological changes in two-dimensional conditions, while also considering structures and hard bottom (non-erodible) areas, to more realistically assess the effects of tsunami-induced sediment transport on the levels of coastal hazard.

ACKNOWLEDGMENTS

REFERENCES

Choowong, M., Murakoshi, N., Hisada, K.-i., Charusiri, P., Charoentitirat, T., Chutakositkanon, V., Jankaew, K., Kanjanapayont, P., and Phantuwongraj, S. (2008). 2004 Indian Ocean tsunami inflow and outflow at Phuket, Thailand. *Marine Geology*, 248(3):179–192.

Elder, J. (1959). The dispersion of marked fluid in turbulent shear flow. *Journal of fluid mechanics*, 5(04):544–560.

Goto, K., Chagué-Goff, C., Goff, J., and Jaffe, B. (2012). The future of tsunami research following the 2011 Tohoku-oki event. *Sedimentary Geology*, 282:1–13.

Grilli, A. and Grilli, S. T. (2013). Modeling of tsunami generation, propagation and regional impact along the upper US East Coast from the Azores convergence zone. Technical Report No. CACR-13-04, Center for Applied Coastal Research, University of Delaware.

Grilli, S. T., Dubosq, S., Pophet, N., Pérignon, Y., Kirby, J. T., and Shi, F. (2010). Numerical simulation and first-order hazard analysis of large co-seismic tsunamis generated in the Puerto Rico trench: near-field impact on the North shore of Puerto Rico and far-field impact on the US East Coast. *Natural Hazards and Earth System Sciences*, 10(10):2109–2125.

Grilli, S. T., O'Reilly, C., Harris, J. C., Tajalli Bakhsh, T., Tehranirad, B., Banihashemi, S., Kirby, J. T., Baxter, C. D. P., Eggeling, T., Ma, G., and Shi, F. (2014). Modeling of SMF tsunami hazard along the upper US East Coast: detailed impact around Ocean City, MD. *Natural Hazards*, 76(2):705–746.

Grothe, P. R., Taylor, L. A., Eakins, B. W., Warnken, R. R., Carignan, K. S., Lim, E., Caldwell, R. J., and Friday, D. (2010). Digital elevation model of ocean city, maryland: Procedures, data and analysis. Technical report, NOAA Technical Memorandum NESDIS NGDC-37, Dept. of Commerce, Boulder, CO, 37 pp.

Hori, K., Kuzumoto, R., Hirouchi, D., Umitsu, M., Janjirawuttikul, N., and Patanakanog, B. (2007). Horizontal and vertical variation of 2004 Indian tsunami deposits: an example of two transects along the western coast of Thailand. *Marine Geology*, 239(3):163–172.

Kirby, J. T., Shi, F., Tehranirad, B., Harris, J. C., and Grilli, S. T. (2013). Dispersive tsunami waves in the ocean: Model equations and sensitivity to dispersion and Coriolis effects. *Ocean Modelling*, 62:39–55.

Kobayashi, N. and Lawrence, A. R. (2004). Cross-shore sediment transport under breaking solitary waves. *Journal of Geophysical Research: Oceans* (1978–2012), 109(C3).

Larson, M. and Kraus, N. C. (1989). Sbeach: numerical model for simulating storm-induced beach change. report 1. empirical foundation and model development. Technical report, DTIC Document.

Shi, F., Kirby, J. T., Harris, J. C., Geiman, J. D., and Grilli, S. T. (2012). A high-order adaptive time-stepping TVD solver for Boussinesq modeling of breaking waves and coastal inundation. *Ocean Modelling*, 43:36–51.

Szczuciński, W., Kokociński, M., Rzeszewski, M., Chagué-Goff, C., Cachão, M., Goto, K., and Sugawara, D. (2012). Sediment sources and sedimentation processes of 2011 Tohoku-oki tsunami deposits on the Sendai Plain, Japan—insights from diatoms, nannoliths and grain size distribution. *Sedimentary Geology*, 282:40–56.

Tanaka, H., Tinh, N. X., Umeda, M., Hirao, R., Pradjoko, E., Mano, A., and Udo, K. (2012). Coastal and estuarine morphology changes induced by the 2011 Great East Japan Earthquake Tsunami. *Coastal Engineering Journal*, 54(01):1250010.

Tehranirad, B., Banihashemi, S., Kirby, J. T., Callahan, J. A., and Shi, F. (2014). Tsunami Inundation Mapping for Ocean City, MD NGDC DEM. Technical Report No, CACR-14-08,

Center for Applied Coastal Research, University of Delaware.

Tehranirad, B., Harris, J. C., Grilli, A. R., Grilli, S. T., Abadie, S., Kirby, J. T., and Shi, F. (2015). Far-Field Tsunami Impact in the North Atlantic Basin from Large Scale Flank Collapses of the Cumbre Vieja Volcano, La Palma. *Pure and Applied Geophysics*, 172(12):3589–3616.

Tehranirad, B., Shi, F., Kirby, J. T., Harris, J. C., and Grilli, S. T. (2011). Tsunami benchmark results for fully nonlinear Boussinesq wave model FUNWAVE-TVD. Version 1.0. Technical Report No. CACR-11-02, Center for Applied Coastal Research, University of Delaware.

Udo, K., Sugawara, D., Tanaka, H., Imai, K., and Mano, A. (2012). Impact of the 2011 Tohoku earthquake and tsunami on beach morphology along the northern Sendai coast. *Coastal Engineering Journal*, 54(01):1250009.

van Rijn, L. C. (1984). Sediment pick-up functions. *Journal of Hydraulic Engineering*, 110(10):1494–1502.

Wilson, R., Davenport, C., and Jaffe, B. (2012). Sediment scour and deposition within harbors in California (USA), caused by the March 11, 2011 Tohoku-oki tsunami. *Sedimentary Geology*, 282:228–240.